Vol. 24 • No. 43 • November 19 • 2014

www.afm-journal.de

ADVANCED FUNCTIONAL MATERIALS

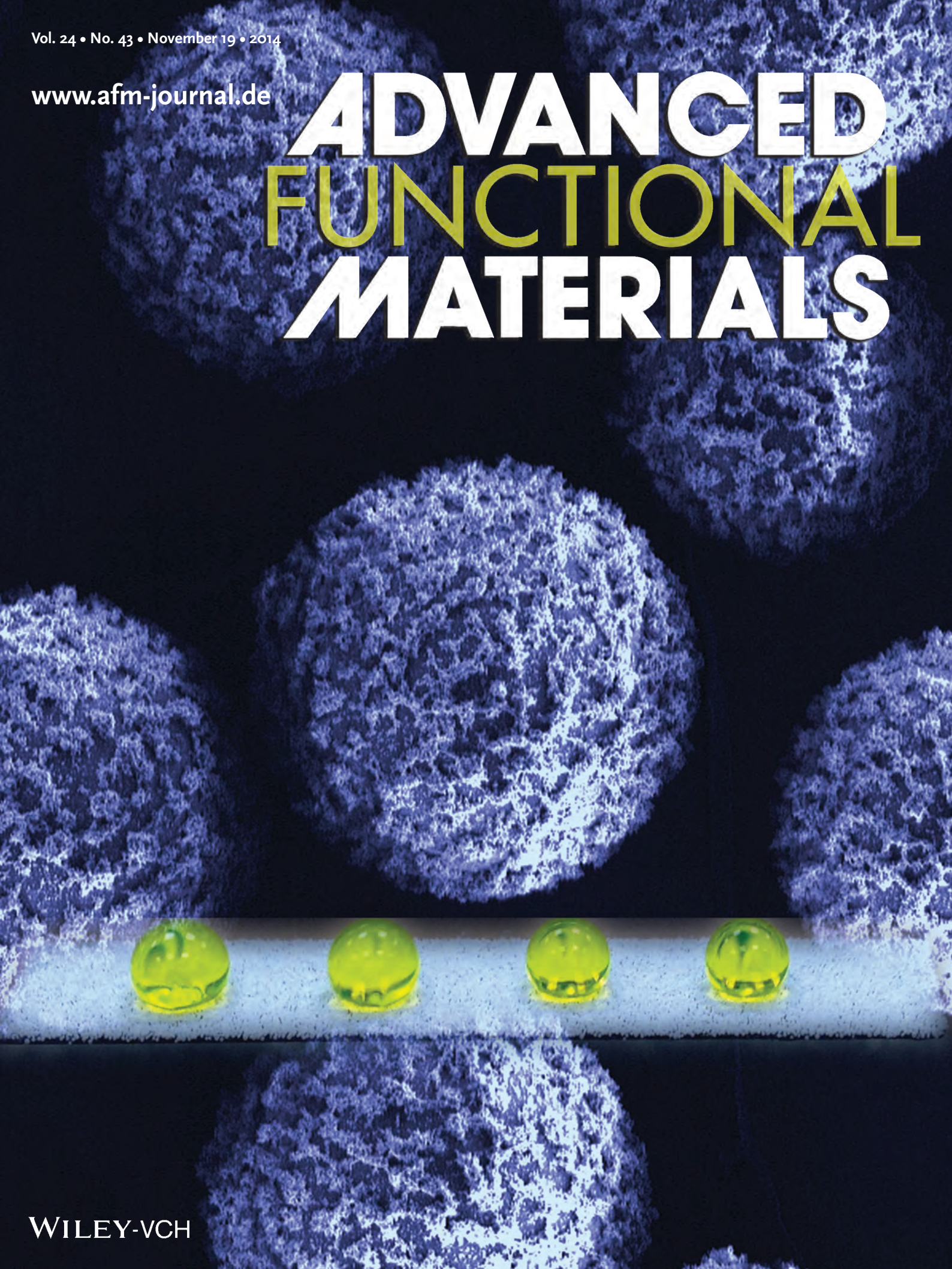

WILEY-VCH

A Versatile Approach towards Multifunctional Robust Microcapsules with Tunable, Restorable, and Solvent-Proof Superhydrophobicity for Self-Healing and Self-Cleaning Coatings

*Gang Wu, Jinliang An, Xiu-Zhi Tang, Yong Xiang, and Jinglei Yang**

Numerous microencapsulation techniques have been developed to encase various chemicals, for which specific processing parameters are required to address the widely differing features of the encapsulated materials. Microencapsulation of reactive agents is a powerful technique that has been extensively applied to self-healing materials. However, the poor solvent compatibility and insufficient thermal stability of microcapsules continue to pose challenges for long-term storage, processing, and service in practical applications. Here, an easily modifiable and highly versatile method is reported for preparing various chemicals filled poly(urea-formaldehyde) microcapsules that exhibit superior tightness against solvents and heat and that possess widely tunable, repetitiously self-restorable, and solvent-proof superhydrophobicity. In addition, the low-cost fabrication of biomimetic multifunctional smart coatings is demonstrated for self-healing anticorrosion and self-cleaning antifouling applications by directly dispersing the superhydrophobic microcapsules into and onto a polymer matrix. The methodology presented in this study should inspire the development of multifunctional intelligent materials for applications in related fields.

1. Introduction

Even the simplest biological system has complex and multifunctional features for autonomous sensing, coordination, reaction, regeneration and healing upon stimulation. Bioinspired materials that exhibit these remarkable smart functions have undergone considerable development recently due to rapid advances in materials science and nanoengineering.[1–6] Among these materials, coatings occupy a special position because they function as an interface between the protected substrate and the external environment and are therefore uniquely suited to multifunctionalization, such as for corrosion protection from external chemical attack, self-healing upon damage, and self-cleaning upon contamination. A well-established approach to realize self-healing in synthetic coating materials is the incorporation of microcapsules (MCs) that contain a healant into the matrix with a catalyst (a two-part formula) or without a catalyst (a one-part formula).[7–11] Although protective coatings are always exposed to harsh environments in which they are subject to temperature fluctuations and attack from water and chemicals, little attention has been given to enhancing shell structures for long-term service and even for storage of the capsules themselves. Existing strategies for improving the resistance of MCs have primarily focused on fabricating a multi-layered shell structure,[12] introducing inorganic nanofillers into the shell,[7,13] and increasing the shell thickness for chemically and physically stable core materials.[14] Thus, the design and preparation of MCs with superior shell tightness to contain reactive species remain extremely challenging for self-healing anticorrosion coating applications.

Coatings are the outermost layer of structures and are therefore continuously subjected to fouling and contamination. The use of micro- and nano-engineered superhydrophobic surfaces can mimic the lotus leaf effect in materials with self-cleaning features.[15–18] A general and successful approach has involved combining specific surfaces with a suitably designed hierarchical structure and low surface-energy materials.[19] However, most of the relevant reports typically involve expensive materials (e.g., perfluoroalkyl silane and nanotubes),[20,21] harsh treatments (such as harsh chemical etching, plasma treatment, chemical vapor deposition, electrodeposition, templating, etc.),[22–26] and multi-step procedures,[27,28] all of which limit the practical applications of these coatings. In addition, the superhydrophobicity of these self-cleaning antifouling surfaces is easily compromised by chemical and physical attack from the surrounding environment. Imbuing long-lasting self-cleaning antifouling coatings with self-restoring superhydrophobicity upon degradation may represent an effective solution to these challenges. Some superhydrophobic coatings or surfaces with healable or regenerative superhydrophobicity have been

Dr. G. Wu, J. An, Dr. X.-Z. Tang, Prof. J. Yang
School of Mechanical and Aerospace Engineering
Nanyang Technological University
Singapore 639798, Singapore
E-mail: mjlyang@ntu.edu.sg
Dr. G. Wu, Prof. Y. Xiang
School of Energy Science and Engineering
University of Electronic Science and Technology of China
Chengdu 610064, China

DOI: 10.1002/adfm.201401473

fabricated.[29–35] However, the reported methods primarily rely on the migration or rearrangement of expensive low-surface-energy components, which are pre-deposited/adsorbed using harsh treatments or multi-step procedures on porous materials, and essential triggering stimuli (i.e., moisture or temperature) for the processes.[36]

Although monofunctional self-healing anticorrosion coatings and self-cleaning antifouling surfaces have been studied extensively, considerable challenges remain for developing bioinspired multifunctional smart coating materials using feasible techniques.[37–40] Herein, we report a facile and low-cost one-pot microencapsulation approach that can be used to efficiently and conveniently prepare multifunctional robust MCs with superior shell tightness and widely tunable, repetitiously self-restorable, and solvent-proof superhydrophobicity for self-healing anticorrosion and self-cleaning antifouling applications. We used in situ polymerization in an oil-in-water emulsion under gentle reaction conditions to successfully prepare a broad range of various reactive or nonreactive liquid cores in resorcinol-modified poly(urea-formaldehyde) (PUF) MCs. The dense and cross-linked shells provided MCs, particularly those with highly reactive liquid cores, with excellent resistance to various organic solvents with low or non-existent polarities and high thermal stabilities up to 150 °C. Notably, the MCs that contained hexamethylene diisocyanate (HDI) as a moisture-sensitive healant[10] possessed an excellent superhydrophobicity that could be widely tunable, self-restorable multiple times, and solvent-proof. Dispersing these HDI-filled MCs into and onto a polymer matrix yielded a multifunctional single coating with concurrent self-healing and self-cleaning features for anticorrosion and antifouling applications; this is the first time that such a coating has been realized.

2. Results and Discussion

2.1. Versatile One-Pot Microencapsulation Method for Preparing MCs with Various Liquid Cores

PUF MCs can be fabricated by a simple preparation procedure and possess a moderate mechanical strength; therefore, PUF MCs have been widely used in the storage of chemical agents with relatively high chemical and physical stabilities under common conditions.[41–43] However, the encapsulation of unstable chemicals with high reactivity and/or volatility by PUF shells remains a challenge. Here, we have successfully achieved a highly efficient microencapsulation of five types of chemical agents using resorcinol-modified PUF as a shell (**Figure 1**). In particular, two highly reactive and volatile liquid agents, HDI and 1H,1H,2H,2H-perfluorooctyltriethoxysilane (POTS), were encapsulated. HDI and POTS are commercial moisture-sensitive chemicals. Thus, the conventional approach of direct in situ polymerization of urea and formaldehyde cannot be employed to encapsulate these two chemicals because of the unstable emulsion that results from their hydrolysis as well as other side reactions occurred between these chemicals and the raw shell materials (e.g., urea and formaldehyde). A UF pre-polymer aqueous solution was first prepared by a commonly used method,[43] and the initial pH of the microencapsulation system was adjusted to 1.55 ± 0.02 with an

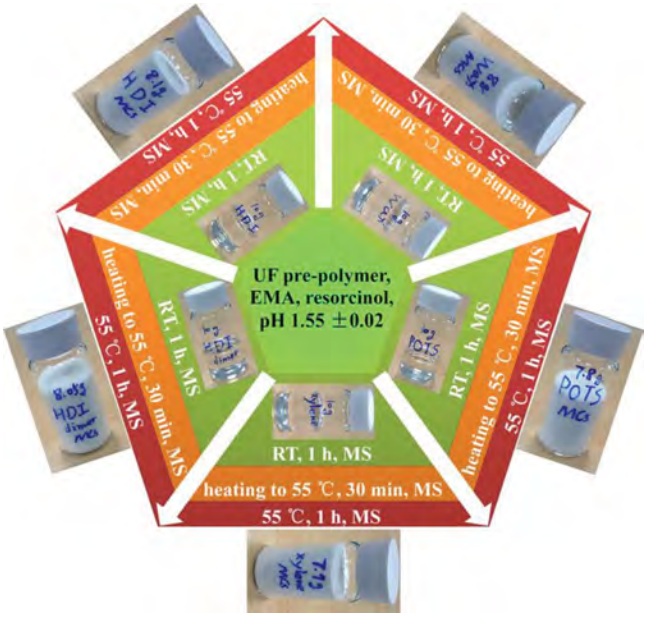

Figure 1. Versatile preparation methods and appearances of various liquid cores and MCs: UF, EMA, and MS denote urea-formaldehyde, poly(ethylene-*alt*-maleic anhydride), and mechanical stirring, respectively.

aqueous solution of citric acid. These two steps accelerated the UF polymerization,[42,44] thereby stabilizing the emulsion by quickly forming an inner shell that isolated the core materials in a water phase and terminated the side reactions. The time for shell formation was reduced from 4 to 1 h.[42]

The resulting MCs were all free-flowing white powders (Figure 1). Scanning electron microscopy (SEM) revealed that the MCs with different cores had very similar structures (**Figure 2**). Common structural features included a regular spherical shape (Figure 2a1, b1, c1, d1, and e1), an approximately 100–350 nm thick dense inner shell (Figure 2a5, b5, c5, d5, and e5), and a hierarchical outer surface structure similar to a lotus leaf surface[18] (Figure 2a2, a3, b2, b3, c2, c3, d2, d3, e2, and e3). According to the mechanism of the in situ polymerization of urea and formaldehyde in water,[42] the formation of hierarchical lotus-leaf-like surface structure is attributed to spontaneous aggregation and deposition of PUF nanoparticles on the capsule surface as the PUF molecular weight increases. In addition, statistical data from 250 MCs in SEM images (Figure S1, Supporting Information) showed that the mean diameters of the MCs with HDI, POTS, wax, and xylene cores, denoted HDI-MCs, POTS-MCs, Wax-MCs, and Xylene-MCs, respectively, were in the 180–200 μm range, whereas the mean diameter of the MCs with HDI dimer core, denoted HDI-D-MCs, was greater than 250 μm and could be attributed to the higher viscosity (152 ± 65 mPa.s at 25 °C) of HDI dimer compared to the other cores. The chemical components of the MCs were characterized by Fourier-transform infrared spectroscopy (FT-IR) (Figure S2, Supporting Information). The spectrum of the capsule core was completely identical to that of the respective pure agent, and clear characteristic signals of the core were observed in the spectra of broken MCs, thereby confirming the successful encapsulation of each agent. In the spectra of the shells, the characteristic signals of the core were not observed,

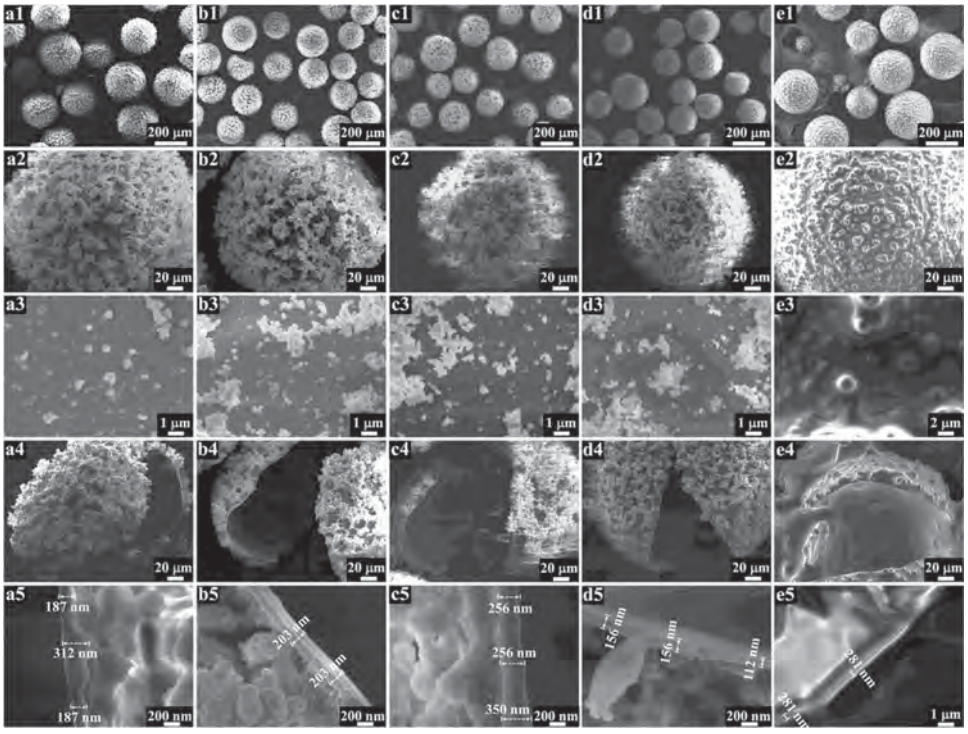

Figure 2. SEM images of MCs with various cores: a1–a5) HDI-MCs; b1–b5) POTS-MCs; c1–c5) Wax-MCs; d1–d5) Xylene-MCs; and e1–e5) HDI-D-MCs.

indicating that no residue of the core remained in the shell; the resorcinol-modified PUF molecular structure was confirmed from the characteristic signals corresponding to the N-H bond, the C = O bond, the N-O bond, and the phenyl-H bond. Thus, this one-pot method of preparing MCs containing various chemicals is simple, efficient, versatile, and economically feasible.

2.2. Solvent Resistance and Thermal Stability of MCs

In practical applications, MCs must be sufficiently robust to survive rigorous environments during the materials processing cycle, such as exposure to solvents, moisture, exothermal reactions, and acids/bases.[12–14,45] However, there are rare reports in the literature of enhanced shell tightness of self-healing microcapsules to solvents and thermal attacks.[7] In this study, the HDI-MCs displayed excellent resistance to weakly polar (xylene and chloroform) and nonpolar (hexane) organic solvents but poor resistance to highly polar solvents (acetonitrile and acetone) at a 2 wt.% concentration over a specified period of time at room temperature. **Figure 3**a shows that the relative released percentage of HDI, as determined by titration, reached a plateau after 48 h of immersion and that the final values after 16 days of immersion in hexane, xylene, and chloroform were 4.13 ± 0.12 wt.%, 3.13 ± 0.12 wt.%, and 10.13 ± 0.12 wt.%, respectively. However, after 24 h of immersion in acetonitrile and 8 h of immersion in acetone, the final value exceeded 90 wt.%. Thus, the solvent resistance was inversely dependent on the solvent polarity, with the exception of acetone. After 16 days of immersion in hexane, xylene, or chloroform, the dried HDI-MCs retained the same structure as the original HDI-MCs (Figure S3, Supporting Information) with a high core content (Figure S4, Supporting Information).

The thermal stability of the resulting MCs was investigated using thermal gravimetric analysis (TGA). The initial evaporation temperature (which was defined at a 5% weight loss) of 136 °C for the freshly prepared HDI-MCs (denoted HDI-MCs-0D) was obviously higher than that of pure HDI (86 °C). The primary weight loss of the HDI-MCs-0D occurred at approximately 250 °C, which corresponded to the first-stage pyrolytic temperature of the shell (Figure 3b), indicating that the MCs possessed excellent thermal stability. The residual weight of the HDI-MCs-0D after this primary weight loss was approximately 10%, corresponding to an encapsulated HDI content of approximately 90%. However, for the broken HDI-MCs-0Ds, the primary weight loss corresponding to the release of HDI was approximately 82%. These results indicate that the actual content of encapsulated HDI was in the 82–90% range, in good agreement with that determined by titration (approximately 85%). After storing the fresh HDI-MCs in a covered glass vial at room temperature for 45 days, the core content was slightly reduced to approximately 78% (Figure 3b), the core component was almost no change (Figure S5, Supporting Information), indicating the long shelf life of the MCs in the sealed vessel. In addition, isothermal experiments with HDI-MCs in a N_2 atmosphere revealed that the residual weights were 89.7% and 73% after heating the MCs for 5 h at 100 °C and 150 °C (Figure 3c), respectively, and the primary weight loss still occurred at approximately 250 °C, indicating a significant improvement in the thermal stability of HDI in the tight-shell capsules compared to pure HDI (Figure S6, Supporting Information). The TGA experiments confirmed the excellent thermal stability

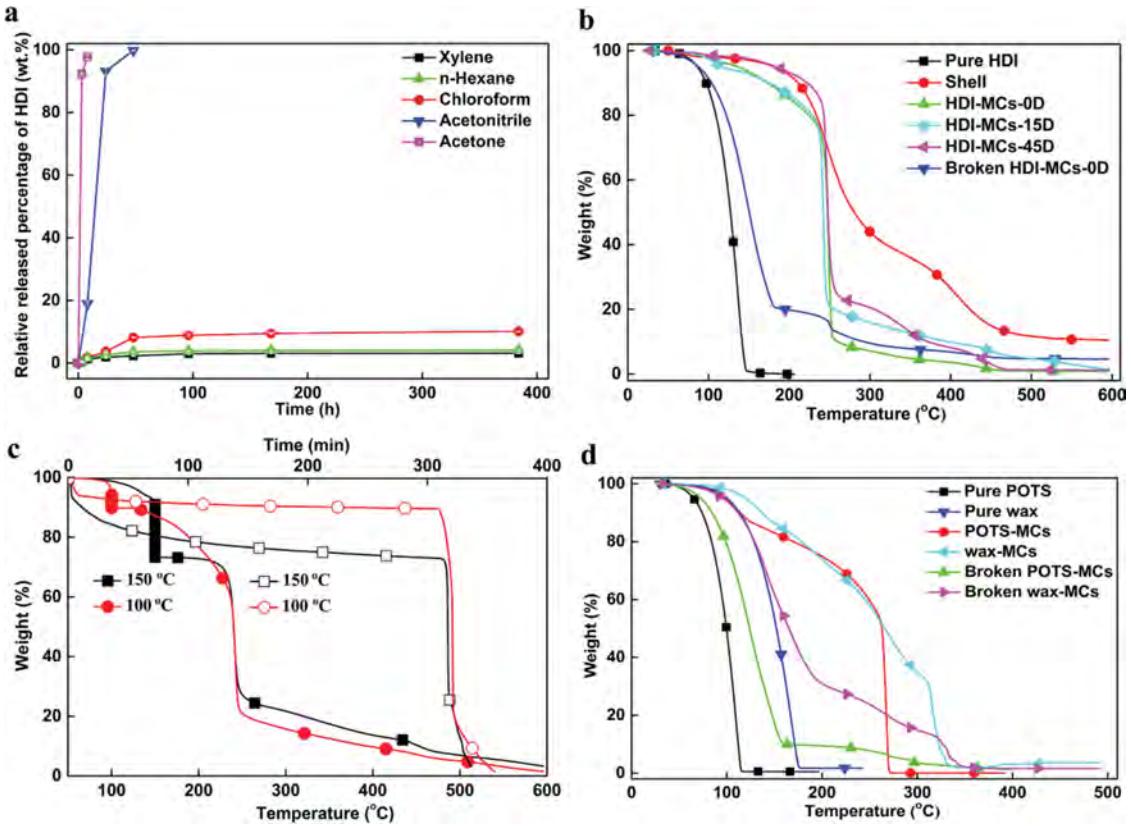

Figure 3. a) Relative released percentage of HDI after immersing HDI-MCs in various organic solvents for different times. b) Thermal gravimetric analysis (TGA) weight loss curves of pure HDI, shell, and HDI-MCs after 0 days (HDI-MCs-0D), 15 days (HDI-MCs-15D), and 45 days (HDI-MCs-45D) of storage and associated broken MCs. c) TGA weight loss curves of HDI-MCs from an isothermal process at 100 °C (○ weight loss as a function of time; ● weight loss as a function of temperature) and 150 °C (□ weight loss as a function of time; ■ weight loss as a function of temperature). d) TGA weight loss curves of pure POTS, pure wax, POTS-MCs, Wax-MCs, and associated broken MCs. All TGA tests were performed at a heat rate of 10 °C min^{-1} in a N_2 atmosphere.

of MCs with different cores, such as POTS-MCs and Wax-MCs (Figure 3d). This tremendous improvement in the thermal stability was primarily attributed to the highly crosslinked shell, which had a superior tightness that prevented the leakage of the liquid core upon heating. The hierarchical surface structure of MCs may also have retarded heat transfer, thereby improving the thermal stability. Differential scanning calorimetry (DSC) experiments clearly demonstrated that the melting range of the Wax-MCs was significantly wider than that of pure wax and increased with the increasing heating rate (Figure S7 and Table S1, Supporting Information).

2.3. Tunable, Self-Restorable, and Solvent-Proof Superhydrophobicity of MCs

Self-cleaning superhydrophobic surfaces can be produced by combining specific surface features with low-surface-energy materials.[19] The SEM observations demonstrated that the resulting MCs had a hierarchical structure (ranging from microns to nanometers in size) on a surface that resembled a lotus leaf. For the POTS-MCs and HDI-MCs, spherical droplets of fluorescein-colored water formed stably on the surfaces of the MCs at room temperature (**Figure 4**a1 and b1), and their water static contact angles (CAs) were 159.5 ± 1.2° and 155.3 ± 0.4°

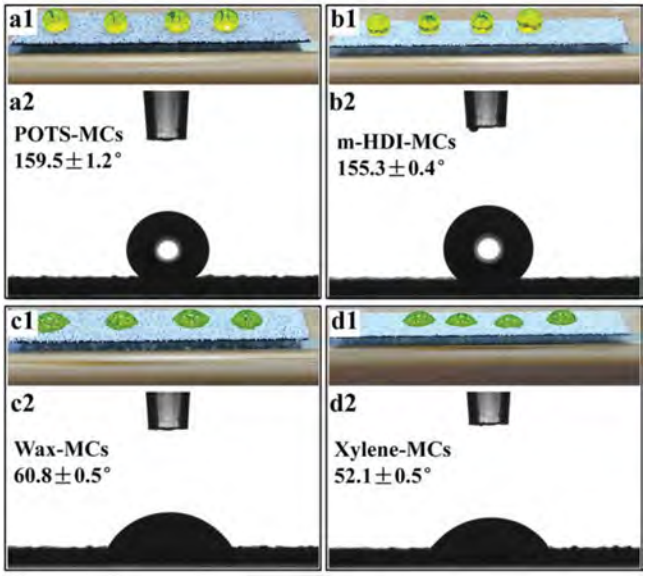

Figure 4. Photos of fluorescein-colored water droplets on the surface of various MCs: a1) POTS-MCs, b1) HDI-MCs, c1) Wax-MCs, and d1) Xylene-MCs. Still images from contact angle (CA) measurements: a2) POTS-MCs, b2) HDI-MCs, c2) Wax-MCs, and d2) Xylene-MCs. MCs were well-dispersed and bonded to the glass slide using double-sided adhesive tape.

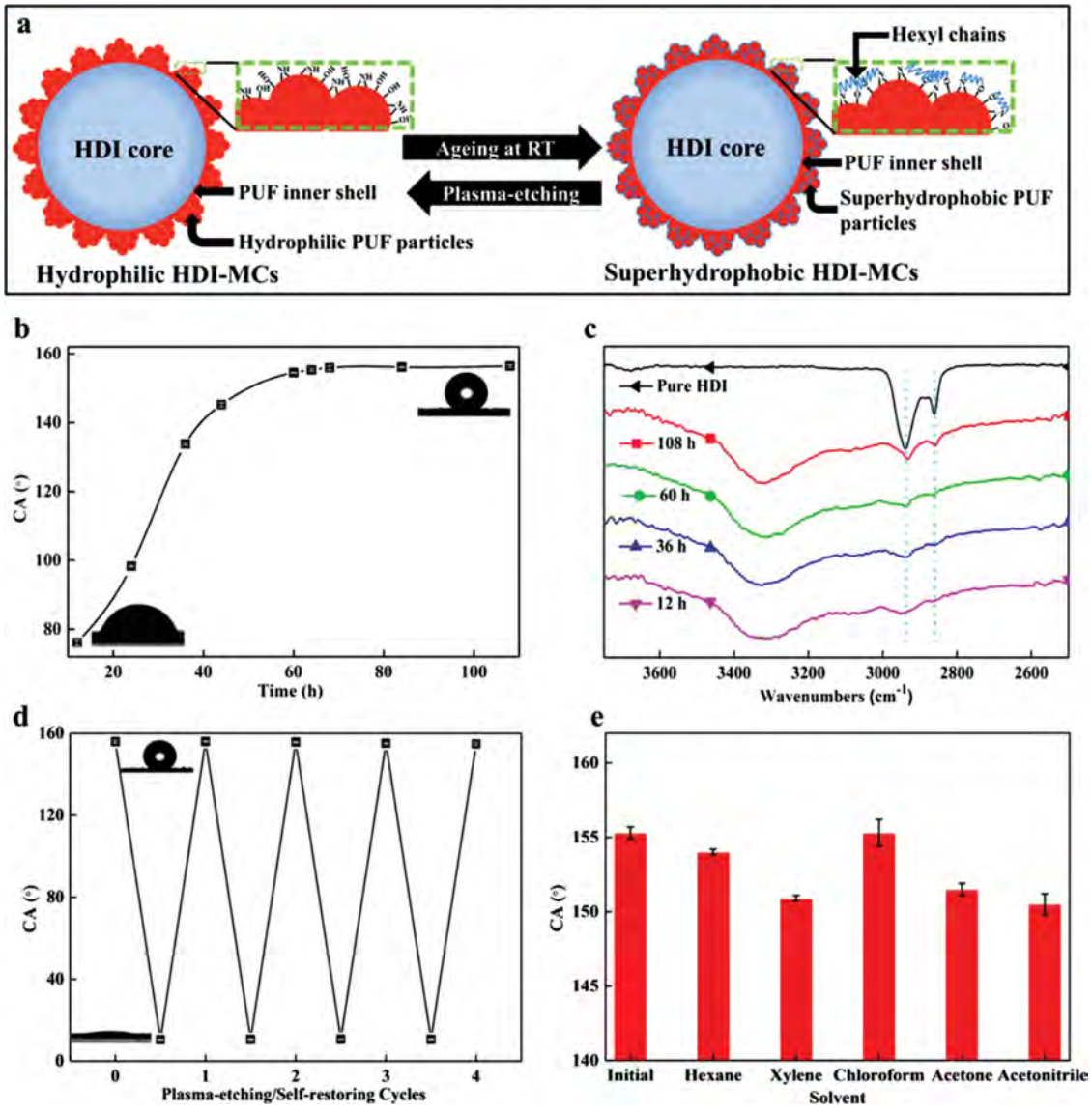

Figure 5. a) Schematic of the mechanism of the reversible hydrophilic-superhydrophobic transition of HDI-MCs. b) Variation in CA with ageing time at room temperature; insets: still CA images of HDI-MCs after 12 h of ageing (bottom left) and 108 h of ageing (top right). c) FT-IR spectra of pure HDI and HDI-MCs shells after ageing at different times. d) Reversible superhydrophobic to hydrophilic transition after plasma-etching and self-restoration cycles at room temperature; insets: still CA images of HDI-MCs after plasma-etching (bottom) and self-restoration (top). e) Superhydrophobicity of HDI-MCs after 16 days of immersion in various organic solvents.

(Figure 4a2 and b2), respectively, demonstrating the superhydrophobicity of the surfaces. However, the Wax-MCs and Xylene-MCs were wetted by water droplets (Figure 4c1 and d1) with the water CAs of 60.8 ± 0.5° and 52.1 ± 0.5° (Figure 4c2 and d2), respectively, demonstrating that the surfaces were hydrophilic. These results are unprecedented; remarkable differences among the water wetting behaviors of these four types of MCs were observed even though their surface features were similar and most of the MCs had low-surface-energy core materials. Note that the POTS and HDI were reactive and volatile, whereas the wax and xylene were nonreactive. Thus, we attributed the generation of superhydrophobicity to inside-out diffusion of the low-surface-energy reactive and volatile core materials and subsequently their spontaneous chemical modification on the MCs surface at room temperature. Indeed, the fresh HDI-MCs were found to be intrinsically hydrophilic due to the presence of abundant hydrophilic groups (e.g., amino and hydroxyl groups) on the PUF particle surface during the formation of PUF MCs (**Figure 5**a),[43] as was the case for the other MCs. The surface gradually changed from hydrophilic to superhydrophobic with time because of the effect of the chemical modification of the diffused HDI, which consumed the hydrophilic groups. After 12 h of ageing at room temperature, the HDI-MCs were typically still hydrophilic, with a CA of 76.1 ± 0.9° (Figure 5b). When the ageing time was prolonged, the CA of the HDI-MCs increased continuously and reached a plateau of approximately 156° after 68 h, corresponding to the time at which superhydrophobicity was achieved. FT-IR attenuated total reflectance

(FT-IR-ATR) spectroscopy of the HDI-MC shell was used to confirm the chemical modification effect. The signals at 2935 cm^{-1} and 2860 cm^{-1} in the spectra, which correspond to the C-H stretching vibration of methylene in the hexyl chains, were enhanced as the ageing time increased (Figure 5c and Figure S8, Supporting Information), implying that HDI diffused out of the shell and reactively bound the shell surface gradually.

The aforementioned mechanism for the creation of superhydrophobicity can be used to explain the differences in the water wetting behavior of the four types of MCs. The PUF shells were intrinsically hydrophilic. The hydrophilic groups of the shell surfaces of the Wax-MCs and Xylene-MCs could not be consumed by nonreactive low-surface-energy core materials. By contrast, for the POTS-MCs and HDI-MCs, the hydrophilic groups of the shell surfaces can be consumed by highly reactive low-surface-energy core materials. Thus, the Wax-MCs and Xylene-MCs can be wetted by water, whereas the surfaces of the POTS-MCs and HDI-MCs thoroughly repelled water. In addition, the superhydrophobicity of the MCs vanished upon removal of the diffused HDI and was self-restorable upon subsequent ageing. To confirm the self-restorability of superhydrophobicity, superhydrophobic HDI-MCs with CA of approximately 156° were etched by O_2 plasma for 2 min, after which the surface became hydrophilic with a CA of approximately 10° (Figure 5d, bottom inset). Then the plasma-etched HDI-MCs were aged at room temperature for 72 h, the superhydrophobicity was restored with a CA of approximately 156° (Figure 5d, top inset). The etching-restoring process could be repeated multiple times without an obvious decrease in the superhydrophobicity (Figure 5d), demonstrating excellent self-restorability. In addition, the superhydrophobicity of the HDI-MCs was maintained after 16 days of immersion in various organic solvents (Figure 5e) with similar CA, indicating excellent solvent stability of the superhydrophobic surfaces.

The superhydrophobicity of the MCs could be easily tuned by adjusting the level of hierarchy of the surface structure. HDI-MCs with low-level, mid-level, and high-level hierarchical structures and smaller diameters were denoted l-HDI-MCs, m-HDI-MCs, h-HDI-MCs, and s-m-HDI-MCs, respectively. These MCs were prepared by varying the formation time and agitation rate of the emulsion (**Table 1** and Figure S9, Supporting Information). The influence of the emulsifying conditions on the levels of hierarchy of the surface structure was attributed to the change of aggregation and deposition of PUF nanoparticles in emulsion. Actually, a long time agitation offering the continuous shearing action was unfavorable for the aggregation and deposition of PUF nanoparticles. Thus, by controlling agitation time in the emulsification stage, the levels of hierarchy of the surface structure can be controlled. The diameters of the l-HDI-MCs, m-HDI-MCs, h-HDI-MCs, and s-m-HDI-MCs were 198.0 ± 28.4 μm, 198.5 ± 32.4 μm, 198.0 ± 31.9 μm, and 105.1 ± 22.4 μm, respectively (Figure S10, Supporting Information). Among these MCs, the l-HDI-MCs had the lowest, thinnest hierarchical structure (**Figure 6**a4 and a5), whereas the h-HDI-MCs had the highest, thickest hierarchical structure (Figure 6c4 and c5). For the l-HDI-MCs, m-HDI-MCs, and h-HDI-MCs, the increase in the level of the hierarchical structure resulted in an increase in the CA from 138.4 ± 0.2° to 160.4 ± 0.9° (Figure 6a1, b1, and c1) and induced a transition in the water wetting state from the Wenzel (penetration) state[46] to the Cassie-Baxter state (suspension)[47] (Figure 6a2, a3, b2, b3, c2, and c3), indicating that the superhydrophobicity of the HDI-MCs could be controlled over a wide range of states. In addition, the levels of the hierarchical structure of the m-HDI-MCs and the s-m-HDI-MCs were similar (Figure 6b4, b5, d4, and d5), but the decrease in the capsule diameter lead to a slight increase in the CA from 155.3 ± 0.4° to 156.6 ± 0.2° (Figure 6b1 and d1) and no change in the water wetting state (Figure 6b2, b3, d2, and d3), indicating that the capsule diameter did not play an important role in controlling superhydrophobicity. Overall, when the size of the HDI-MCs was fixed, increasing the level of the hierarchical structure on the surfaces of the HDI-MCs (Figure 6a6, b6, and c6) dramatically increased the CA and changed the water wetting state from the Wenzel state to the Cassie-Baxter state, whereas for HDI-MCs with similar surface hierarchical structures (Figure 6b6 and d6), the difference in size had no obvious effect on the CA.

2.4. Self-Healing and Self-Cleaning Multifunctional Coating Based on HDI-MCs

HDI reacts with water or moisture to generate unstable intermediate carbamic acids that decompose to amines, which in

Table 1. Processing parameters for MCs with different core materials and structures.[a)]

MC Code	Core material	Emulsification agitation rate [rpm]	Emulsification time [min]	Mean diameter [μm]
POTS-MC	POTS	700	20	185.5 ± 25.2
Wax-MC	wax	800	20	184.5 ± 25.6
Xylene-MC	xylene	600	20	183.2 ± 24.8
HDI-D-MC	HDI dimer	1000	20	251.0 ± 81.8
l-HDI-MC[b)]	HDI	600	30	198.0 ± 28.4
HDI-MC/m-HDI-MC[b)]	HDI	600	20	198.5 ± 32.4
h-HDI-MC[b)]	HDI	600	10	198.0 ± 31.9
s-m-HDI-MC[b)]	HDI	800	20	105.1 ± 22.4

[a)]For all of the MCs, the chemical dosage, reaction conditions and processing procedures were completely identical to those for HDI-MC; [b)]l, m, and h in the MCs denote the hierarchical structure on the MC surface corresponded to a low, medium, and high level, respectively, s denotes a small MC.

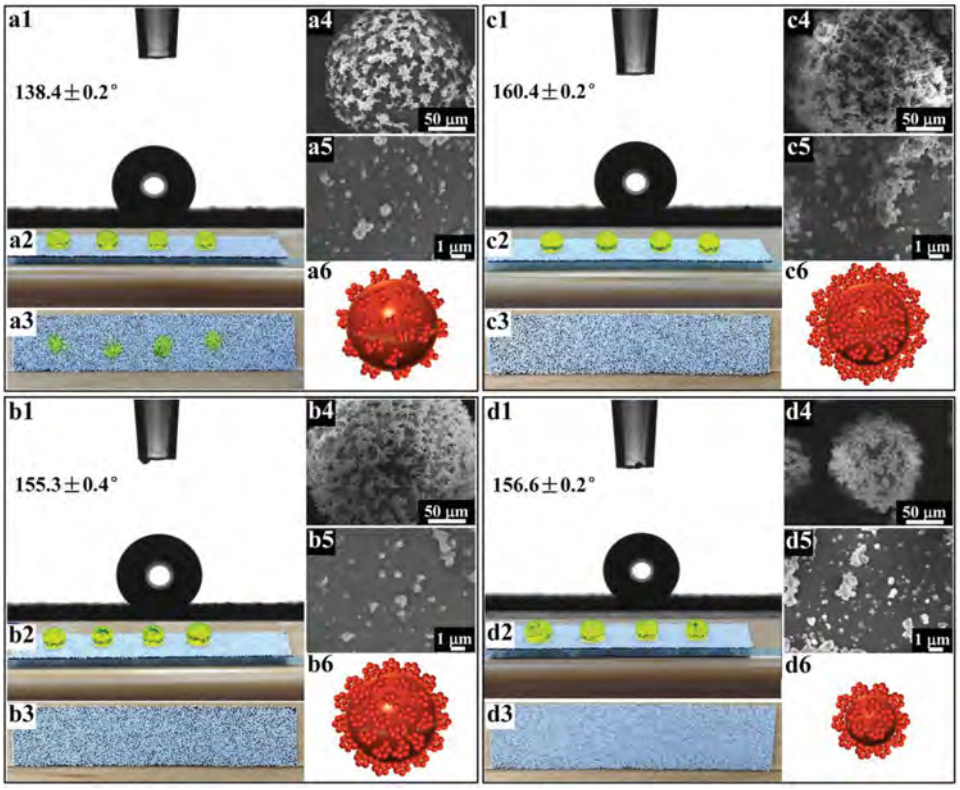

Figure 6. Still CA images of a1) l-HDI-MCs, b1) m-HDI-MCs, c1) h-HDI-MCs, and d1) s-m-HDI-MCs. Photos of fluorescein-colored water droplets on the surface of MCs: a2) l-HDI-MCs, b2) m-HDI-MCs, c2) h-HDI-MCs, and d2) s-m-HDI-MCs. Photos of the surfaces of a3) l-HDI-MCs, b3) m-HDI-MCs, c3) h-HDI-MCs, and d3) s-m-HDI-MCs after removing fluorescein-colored water droplets. Microstructures of HDI-MCs: a4, a5) l-HDI-MCs, b4, b5) m-HDI-MCs, c4, c5) h-HDI-MCs, and d4, d5) s-m-HDI-MCs. Illustrations of the hierarchical surface structures of the individual MCs: a6) l-HDI-MCs, b6) m-HDI-MCs, c6) h-HDI-MCs, and d6) s-m-HDI-MCs.

turn react with other HDI molecules to form polyureas. Thus, the design and development of multifunctional coatings based on HDI-MCs are of significant technical and economic importance for anticorrosion and antifouling applications.

Herein, a unique multifunctional coating that seamlessly integrates antifouling and anticorrosion features was facilely prepared by embedding HDI-MCs into an epoxy matrix coated onto a 50 mm × 50 mm steel panel and binding HDI-MCs powders onto this cured epoxy surface (**Figures 7**a and b1 left). Epoxy coating with embedded HDI-MCs solely and pure epoxy coating of the same thicknesses covering steel panels of the same size were prepared as controls (Figure 7b1, middle and right, respectively). The CAs of the control specimens were less than 90°, clearly indicating hydrophilic surfaces. However, the CA of the multifunctional coating was 163.6 ± 0.3°, revealing that a remarkably superhydrophobic surface. Water droplets rolled off rapidly on that surface tilted by 5.5° within about 0.2 s (Figure S11, Supporting Information). These results demonstrated that our multifunctional coating simultaneously had a very high water static CA and a very low sliding angle (SA), which indicated potential self-cleaning ability. Natural dusts used as dirt were overlaid onto the coatings that were tilted by less than 10°. Water was dropped at higher end and the dusts were then efficiently and completely rolled down together with the water droplets from the multifunctional coating surface. However, the dirt particles on the surface of the control coatings were not removed (Figure 7b1–b4 and Video S1, Supporting Information). This self-cleaning feature is attributed two fundamental mechanisms as mentioned: i.e. the weak interaction of the coating with the water droplets and the easy rolling of the water droplets containing the contaminants down the coating. The HDI-MCs were partially embedded in the epoxy matrix (Figure 7e), and the protruding parts of the HDI-MCs provided a superhydrophobic rough surface that enabled the water droplets in the Cassie-Baxter state to roll off freely, thereby removing the contaminants. This is the first report of the fabrication of a self-cleaning coating by directly binding superhydrophobic MCs onto epoxy coating without any further surface treatment.

To evaluate the anticorrosion performance, pure epoxy coating and multifunctional coating were manually scratched using a razor blade (Figure 7c1 and c3), followed by the immersion of the specimens in a 10 wt.% NaCl aqueous solution at room temperature for 48 h. After immersion, the scratched areas of the multifunctional coating were almost completely free of rust (Figure 7c4). By contrast, significant amount of rust was observed on the control specimen (Figure 7c2). No visible corrosion was observed on the steel panel after peeling off the self-healing coating (Figure S12b), whereas severe corrosion occurred on the steel panel of the control specimen (Figure S12a). These results clearly demonstrate that the multifunctional coating provided excellent corrosion protection for the scratched steel panel. The anticorrosion performance

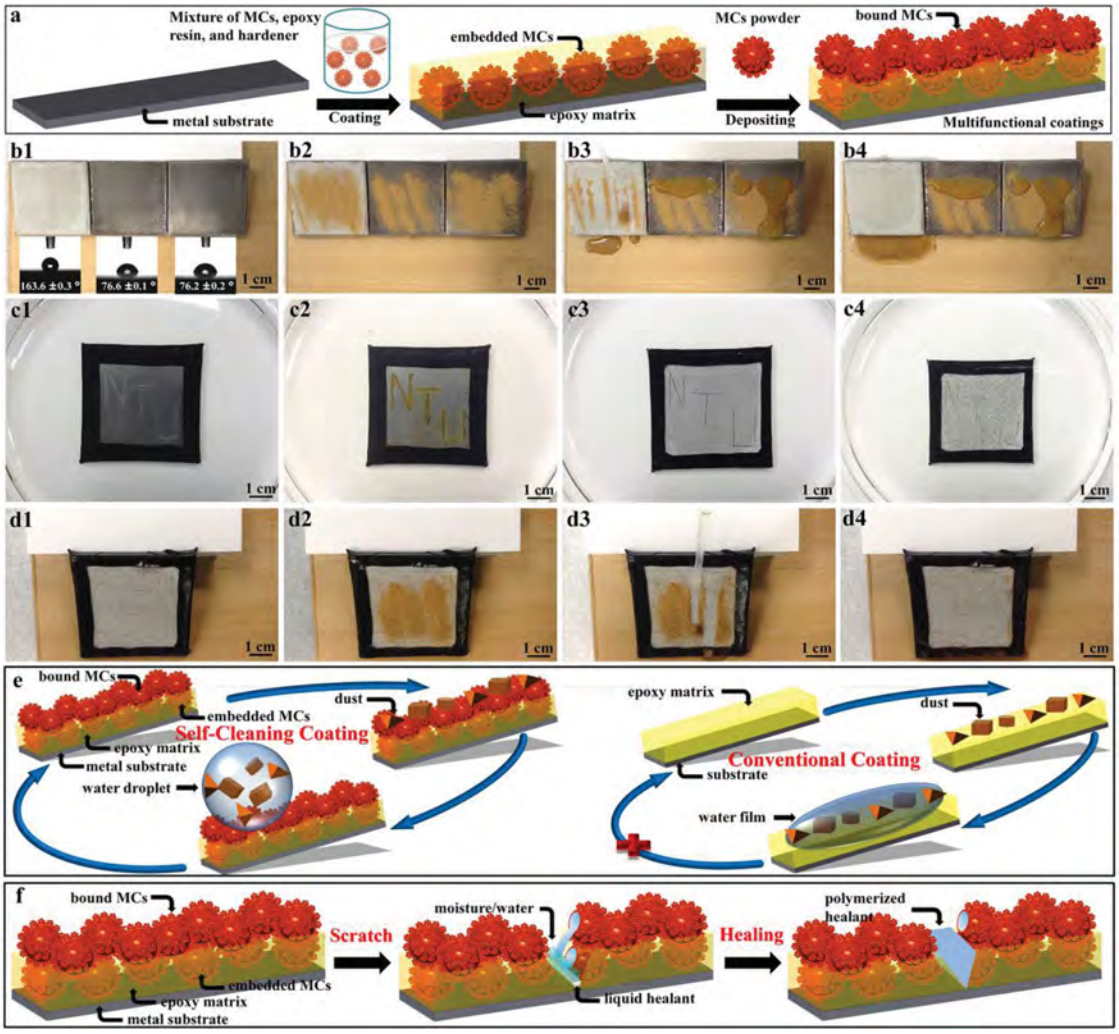

Figure 7. a) Schematic of the preparing procedure of multifunctional coatings. b1–b4) Photos of an antifouling experiment using steel panels covered by different epoxy coatings, in which deionized water was used as a liquid and natural dusts were used as dirt (insets in a show still images from the CA test on steel panels covered by different epoxy coatings): epoxy coatings with embedded/bound HDI-MCs (left), epoxy coatings with embedded HDI-MCs (middle), and pure epoxy coatings (right). Photos of a self-healing anticorrosion experiment using steel panels covered by different epoxy coatings: pure epoxy coating c1) before and c2) after 48 h immersion, epoxy coating with embedded/bound HDI-MCs c3) before and c4) after 48 h immersion. d1–d4) Photos of the self-cleaning antifouling experiment: the specimen was a steel panel covered with an epoxy coating with embedded/bound HDI-MCs, which was fabricated in a self-healing anticorrosion experiment with 48 h of immersion. e) Schematic of the self-cleaning and non-self-cleaning processes. f) Schematic of the self-healing process.

was attributed to the multifunctional coating's self-healing function, which was realized by the released liquid healant (HDI) from the damaged areas that reacted with moisture or water to form a polymerized product (polyurea) to fill the crack (Figure 7f). Thus, the crack is sealed autonomously to retard the diffusion of salt ions, thereby protecting the substrate from corrosion. This mechanism is supported by SEM observations, which revealed that the cracks on the top (Figures S13a and S13b) and bottom (Figures S13c and S13d) surfaces of the scratched areas of the self-healing coating were repaired by the newly formed material. The healing behavior of our multifunctional coatings was completely autonomous and did not require any external intervention such as UV exposure, heating, or the use of a catalyst or other assisting chemicals, enhancing the convenience of developing self-healing anticorrosion coatings of considerable technical and commercial importance.

After 48 h of immersion, the multifunctional coating was washed with acetone, dried in the open air, and tilted by less than 15° to assess the self-cleaning ability (Figure 7d1). Natural dusts were overlaid on the surface of coatings (Figure 7d2). Then, water was added dropwise. The dusts covered the water droplets and were almost completely removed from the coating surfaces by the rolling of the water droplets along the surface (Figure 7d3 and d4, and Video S2, Supporting Information), indicating that the self-cleaning ability was retained. Remarkably, water droplets also rolled off the scratched areas, implying that this type of physical damage did not result in a severe loss of the self-cleaning ability. This is the first report of the fabrication of single polymer coating with both self-cleaning and

self-healing functions for an integrated antifouling and anticorrosion application.

3. Conclusions

We have presented a simple and versatile strategy for synthesizing robust MCs containing various core materials with superior resistance to solvents and excellent thermal stability. Using a modified one-pot in situ polymerization of an oil-in-water emulsion under a shorter reaction time (1 h at 55 °C) than that used in previous reports (at least 4 h at 55 °C), five types of pure liquid agents, including highly reactive and volatile liquid chemicals (i.e., HDI and POTS), were encapsulated successfully and efficiently in a PUF shell. The dense and highly crosslinked PUF shell provided the resulting MCs, particularly those with a highly reactive liquid core (i.e., HDI), with a long shelf life (i.e., the core content was reduced by approximately 10% after the MCs were placed in a sealed vessel for 45 days), and the MCs exhibited excellent resistance to a variety of less polar and nonpolar organic solvents as well as outstanding thermal stability. Thus, our microencapsulation approach could be used to fabricate MCs containing other core materials with functional fillers with desirable properties for extensive applications.

The process parameters were finely tuned to develop a similar approach for constructing a controllable hierarchical surface structure on MCs with reactive cores (i.e., POTS and HDI) with tunable, multiple self-restorable, and solvent-proof superhydrophobicity. The FT-IR-ATR spectra and time-dependent CA were used to develop a mechanism of superhydrophobicity, i.e., the spontaneous chemical modification of low-surface-energy reactive and volatile core materials onto the hierarchical surface of MCs by diffusion, which was verified by the observation of a cyclic hydrophilic-superhydrophobic transition for plasma-etching and ageing processes. This phenomenon opens up a new field of acquiring regenerative superhydrophobicity.

Our superhydrophobic MCs with reactive cores have many promising energy, environmental, and biomedical applications. As an example, a multifunctional smart coating for anticorrosion and antifouling applications was developed using self-healing and self-cleaning mechanisms, respectively, by dispersing an epoxy with HDI-MCs mixed into the matrix onto a surface. The surface MCs exhibited a significant antifouling effect because of their superhydrophobic characteristics. The coated body exhibited excellent anticorrosion performance upon scratching due to healing by the released HDI. This is the first report of a multifunctional single coating with the seamlessly combined anticorrosion and antifouling properties.

4. Experimental Section

Materials: The following chemicals were purchased from Sigma-Aldrich: HDI, resorcinol, 37 wt.% aqueous solution of formaldehyde, 0.1 mol L^{-1} aqueous solution of hydrochloric acid, bromophenol blue, NaCl, anhydrous *p*-xylene, anhydrous n-hexane, anhydrous chloroform, acetone (water <0.1%), anhydrous acetonitrile, citric acid, and fluorescein. POTS was purchased from Alfa Aesar. The HDI dimer (Desmodur® N 3400) was obtained from Bayer MaterialScience. Wax (EPISOL B 2538, C14-C17) was obtained from International Pte., Ltd. Ethylene-maleic anhydride (EMA) copolymer was purchased from MP Biomedicals. The epoxy resin (EPOLAM 5015) and hardener (EPOLAM 5015) were obtained from Axson. The sodium hydroxide aqueous solution (1 mol L^{-1}) and the aqueous solution of hydrochloric acid (1 mol L^{-1}) were purchased from VWR International Ltd. Glass slides (SailBoat Lab Co., Ltd., China) with dimensions of 25.4 mm × 76.2 mm and steel panels (from the local market in Singapore) with dimensions of 50 mm × 50 mm were used as substrates. Natural dusts (<180 μm in size) were obtained from the NTU campus and used as dirt. All of the chemicals in this study were used without further purification unless otherwise specified.

Measurements: The structure of the MCs and the scribed areas of the self-healing coatings were observed by scanning electron microscopy (using a JEOL JSM-7600F and a JSM-5600LV, respectively). All of the samples were fixed onto carbon conductive adhesive tape and coated with gold. The mean diameter and size distribution of the MCs were obtained from the statistical data for 250 MCs of SEM images analyzed using Image-Pro Plus 6.0. The chemical components of the MCs were detected by Fourier transform-infrared spectroscopy (FT-IR, Nicolet 6700, Thermo Fisher Scientific Inc.) on an instrument equipped with an ATR accessory. Observations were made in the 500 cm^{-1} to 4000 cm^{-1} range of the spectrum. For the FT-IR spectra of the pure shell and core, small amounts of MCs were crushed and washed with acetone 5–7 times. After filtering and drying the samples, pure core and shell samples were obtained for analysis. The thermal properties of the samples were characterized by thermal gravimetric analysis (TGA, Q500, TA Instruments) and differential scanning calorimetry (DSC, Q200, TA Instruments). Static contact angle (CA) and slide angle (SA) measurements were obtained using an Attension Theta system (KSV Instruments Ltd.) and recorded using a digital camera with the calculation software supplied. For the CA measurements, 5 μL of deionized water was used, and every sample was measured at least three different points to obtain an average CA and its standard deviation. For the SA measurements, 10 μL of deionized water and a self-made tilting table were used. All photos and videos were recorded with a digital camera.

Preparation of MCs: The resorcinol-modified PUF MCs with various cores were prepared by in situ polymerization. The typical experimental procedure for preparing HDI-MCs was as follows: first, 6.33 g of 37 wt.% aqueous solution of formaldehyde (78.0 mmol) adjusted to pH 8 ± 0.02 with 1 mol L^{-1} NaOH was added to 2.5 g urea (41.6 mmol) in a 20-ml vial. The vial was placed in a temperature-controlled water bath at a preset temperature of 70 °C for 60 min under magnetic stirring, after which the reaction was stopped, and a urea-formaldehyde pre-polymer aqueous solution was obtained. Second, 0.25 g of resorcinol (2.3 mmol), 16.4 g of 2.5 wt.% EMA aqueous solution, and 45.6 g of DI water were added to a 250 ml beaker. The aforementioned pre-polymer solution was added to the mixture using a digital mixer (Caframo) driving a three-bladed propeller at a gentle agitation rate of 200 rpm at 22 °C, resulting in a water phase with a final EMA concentration of approximately 0.5 wt.%. The pH of the system was then adjusted to 1.55 ± 0.02 using an aqueous solution of citric acid (pH ≃ 0.86). Then, the stirring rate was increased to 600 rpm, and 10 g of HDI (59.4 mmol) was added dropwise to the solution. The system was emulsified at 22 °C for 20 min at 600 rpm. The stirring rate was decreased to 200 rpm, and the system was further stirred for 40 min at 22 °C. The system was then heated to 55 °C over approximately 30 min and further reacted for 60 min at 55 °C. The reaction was stopped by cooling the system to room temperature (RT). The MCs were washed 5 times with deionized water, filtered, and air-dried at RT for 12 h before further analysis. The resulting MCs, which weighed approximately 8.1 g, were denoted m-HDI-MCs. By adjusting the reaction time or the agitation rate of the emulsification process in the aforementioned experimental procedure, POTS-MCs, Wax-MCs, Xylene-MCs, HDI-D-MCs, and HDI-MCs with different structures were prepared. The detailed experimental parameters are summarized in Table 1.

Thermal Resistance and Core Fraction of MCs: The thermal resistance and core fraction of MCs were characterized by TGA. The typical

experimental procedure was as follows: approximately 10 mg of sample was placed in a platinum pan and heated to a specified temperature under a N_2 atmosphere at a rate of 10 °C min^{-1} or was maintained for a fixed time at 100 °C and 150 °C in an N_2 atmosphere. The core fraction of the MCs was roughly estimated from the peak width of the derivative of the weight loss curve.

Solvent Resistance of MCs: The resistance of the MCs with an HDI core to various organic solvents was assessed using an immersion test. The typical experimental procedure was as follows: 0.2 g of HDI-MCs was immersed in 10 g of anhydrous *p*-xylene, anhydrous n-hexane, anhydrous chloroform, anhydrous acetonitrile, or acetone for a fixed time at RT. Then, 2 g of the upper clear liquid was absorbed and titrated by a standard method, i.e., ASTM D2572–97. Each sample was titrated three times in parallel to obtain the average relative released percentage of HDI and its standard deviation. The relative released percentage of HDI encapsulated in the MCs (HDI_{RRP} wt.%) was calculated as follows:

$$HDI_{RRP}\ wt.\% = \frac{m_{(HDI\ released)}}{m_{(HDI\ encapsulated)}} \times 100\% \quad (1)$$

$$m_{(HDI\ released)} = 2 \times m_{solvent} \times \frac{NCO\%}{1\text{-}NCO\%} \quad (2)$$

$$NCO\% = \frac{(V_{blank} - V) \times C_{HCl} \times 0.042}{m_{specimen}} \times 100\% \quad (3)$$

where NCO% is the weight percentage of NCO released into the solvent, V_{blank} (ml) is the volume of the standard HCl aqueous solution consumed by the blank, V (ml) is the volume of the standard HCl aqueous solution consumed by 2 g of the specimen, C_{HCl} (mol l^{-1}) is the normality of the standard HCl aqueous solution, 0.042 is the milliequivalent weight of the NCO group, $m_{specimen}$ (g) is the weight of the specimen (2 g), $m_{(HDI\ released)}$ (g) is the released weight of HDI for the total weight of the MCs, $m_{solvent}$ (g) is the weight of the solvent (10 g), and $m_{(HDI\ encapsulated)}$ (g) is the total weight of HDI encapsulated in 0.2 g of MCs.

Plasma Treatment of HDI-MCs: The superhydrophobic HDI-MCs were subjected to oxygen plasma treatment using a March PX-500 plasma system (MARCH Instruments Incorporated). A treatment time of 2 min at 0.27 mbar under a power of 90 W was used. The plasma treatment was used to convert superhydrophobic HDI-MCs into hydrophilic HDI-MCs. However, the superhydrophobicity of the HDI-MCs was completely self-restored after 72 h of ageing at RT.

Preparation and Evaluation of the Multifunctional Coating: The typical experimental procedure for fabricating the self-healing, self-cleaning coating was as follows: first, at RT, 5 g of epoxy resin was mixed with 0.72 g of HDI-MCs and 1.5 g of hardener in sequence; the mixture was then degassed with approximately 10 wt.% of HDI-MCs for 10 min under vacuum. Meanwhile, steel panels with dimensions of 50 mm × 50 mm were polished using sand paper (with a grain size of 350–400), degreased by acetone, and washed with deionized water. After drying, the steel panels were coated by the aforementioned degassed mixture to an average thickness of 300 ± 20 μm. After complete curing at RT, the epoxy layer embedded with HDI-MCs was recoated using a degassed mixture of 5 g of epoxy resin and 1.5 g of hardener to an average thickness of 50 ± 10 μm, after which the other HDI-MCs were uniformly deposited onto this fresh epoxy layer. After a second epoxy layer was completely cured at RT, the surface of the coatings was blown with an air gun to remove unbound MCs. Control specimens of pure epoxy coatings and epoxy coatings embedded with HDI-MCs with the same thicknesses and sizes were prepared and treated in the same manner for comparison. To evaluate self-cleaning antifouling, specimens with a tilt angle of approximately 8° were covered using natural dusts as dirt, followed by the dropwise addition of deionized water to the surface of the specimens. The self-cleaning process was recorded with a digital camera. To evaluate self-healing anticorrosion, the uncoated areas of the steel panels were covered by waterproof adhesive tape, and a razor blade was used to scratch the surface manually. These specimens were immersed in a 10 wt.% NaCl solution at RT for 48 h to evaluate the accelerated corrosion process. The corrosion characteristics were recorded using a digital camera. The scribed areas were inspected by SEM to examine the self-healing performance of the coating.

Supporting Information

Supporting Information is available from the Wiley Online Library or from the author.

Acknowledgements

This work was financially supported by the Ministry of Education of Singapore (Grant #: RG17/09) and National Research Foundation of Singapore (Grant #: NRF2011NRF-POC002–044)

Received: May 7, 2014
Revised: July 8, 2014
Published online: August 22, 2014

[1] L. J. Bonderer, A. R. Studart, L. J. Gauckler, *Science* **2008**, *319*, 1069.
[2] M. Darder, P. Aranda, E. Ruiz-Hitzky, *Adv. Mater.* **2007**, *19*, 1309.
[3] T. S. Wong, S. H. Kang, S. K. Tang, E. J. Smythe, B. D. Hatton, A. Grinthal, J. Aizenberg, *Nature* **2011**, *477*, 443.
[4] M. E. McConney, K. D. Anderson, L. L. Brott, R. R. Naik, V. V. Tsukruk, *Adv. Funct. Mater.* **2009**, *19*, 2527.
[5] A. R. Studart, *Adv. Mater.* **2012**, *24*, 5024.
[6] A. J. Scardino, R. de Nys, *Biofouling* **2011**, *27*, 73.
[7] G. Wu, J. An,D. Sun, X.-Z. Tang,Y. Xiang, J. Yang, *J. Mater. Chem. A* **2014**, *2*, 11614.
[8] S. R. White, N. R. Sottos, P. H. Geubelle, J. S. Moore, M. R. Kessler, S. R. Sriram, E. N. Brown, S. Viswanathan, *Nature* **2001**, *409*, 794.
[9] H. Jin, C. L. Mangun, A. S. Griffin, J. S. Moore, N. R. Sottos, S. R. White, *Adv. Mater.* **2014**, *26*, 282.
[10] M. Huang, J. Yang, *J. Mater. Chem.* **2011**, *21*, 11123.
[11] M. Huang, J. Yang, *Progr. Org. Coating* **2014**, *77*, 168.
[12] M. M. Caruso, B. J. Blaiszik, H. Jin, S. R. Schelkopf, D. S. Stradley, N. R. Sottos, S. R. White, J. S. Moore, *ACS Appl. Mater. Interfaces* **2010**, *2*, 1195.
[13] C. Fan, X. Zhou, *Polym. Adv. Technol.* **2009**, *20*, 934.
[14] Q. Li, A. K. Mishra, N. H. Kim, T. Kuila, K. Lauc, J. H. Lee, *Compos. Part B* **2013**, *49*, 6.
[15] W. Barthlott, C. Neinhuis, *Planta* **1997**, *202*, 1.
[16] I. P. Parkin, R. G. Palgrave, *J. Mater. Chem.* **2005**, *15*, 1689.
[17] V. A. Ganesh, H. K. Raut, A. S. Nair, S. A. Ramakrishna, *J. Mater. Chem.* **2011**, *21*, 16304.
[18] J. Zhang, A. Wang, S. Seeger, *Adv. Funct. Mater.* **2014**, *24*, 1074.
[19] R. Blossey, *Nat. Mater.* **2003**, *2*, 301.
[20] Y. K. Lai, Y. X. Tang, J. J. Gong, D. G. Gong, L. F. Chi, C. J. Lin, Z. Chen, *J. Mater. Chem.* **2012**, *22*, 7420.
[21] S. Srinivasan, V. K. Praveen, R. Philip, A. Ajayaghosh, *Angew. Chem. Int. Ed.* **2008**, *47*, 5750.
[22] Y. A. Dai, H. C. Chang, K. Y. Lai, C. A. Lin, R. J. Chung, G. R. Lin, J. H. He, *J. Mater. Chem.* **2010**, *20*, 10924.
[23] S. H. Kim, J.-H. Kim, B.-K. Kang, H. S. Uhm, *Langmuir* **2005**, *21*, 12213.
[24] X. Deng, L. Mammen, Y. Zhao, P. Lellig, K. Müllen, C. Li, H.-J. Butt, D. Vollmer, *Adv. Mater.* **2011**, *23*, 2962.
[25] N. Zhao, F. Shi, Z. Wang, X. Zhang, *Langmuir* **2005**, *21*, 4713.
[26] W.-L. Min, B. Jiang, P. Jiang, *Adv. Mater.* **2008**, *20*, 3914.
[27] Z. Z. Luo, Z. Z. Zhang, L. T. Hu, W. M. Liu, Z. G. Guo, H. J. Zhang, W. J. Wang, *Adv. Mater.* **2008**, *20*, 970.

[28] Y. Jung, B. Bhushan, *ACS Nano* **2009**, *3*, 4155.
[29] Y. Li, L. Li, J. Sun, *Angew. Chem. Int. Ed.* **2010**, *49*, 6129.
[30] H. Wang, Y. Xue, J. Ding, L. Feng, X. Wang, T. Lin, *Angew. Chem. Int. Ed.* **2011**, *50*, 11433.
[31] Q. Liu, X. Wang, B. Yu, F. Zhou, Q. Xue, *Langmuir* **2012**, *28*, 5845.
[32] U. Manna, D. M. Lynn, *Adv. Mater.* **2013**, *25*, 5104.
[33] H. Zhou, H. Wang, H. Niu, A. Gestos, T. Lin, *Adv. Funct. Mater.* **2013**, *23*, 1664.
[34] J. Wu, J. Li, B. Deng, H. Jiang, Z. Wang, M. Yu, L. Li, C. Xing, Y. Li, *Sci. Rep.* **2013**, *3*, 2951.
[35] A. C. C. Esteves, Y. Luo, M. W. P. van de Put, C. C. M. Carcouët, G. de With, *Adv. Funct. Mater.* **2014**, *24*, 986.
[36] C. H. Xue, J. Z. Ma, *J. Mater. Chem. A* **2013**, *1*, 4146.
[37] J. P. Youngblood, N. R. Sottos, *MRS Bull.* **2008**, *33*, 732.
[38] D. Shchukin, H. Möhwald, *Science* **2013**, *341*, 1458.
[39] Z. Zheng, X. Huang, M. Schenderlein, D. Borisova, R. Cao, H. Möhwald, D. Shchukin, *Adv. Funct. Mater.* **2013**, *23*, 3307.
[40] X. Wang, Y. Wang, S. Bi, Y. Wang, X. Chen, L. Qiu, J. Sun, *Adv. Funct. Mater.* **2014**, *24*, 403.
[41] K. Dietrich, H. Herma, R. Nastke, E. Bonatz, W. Teige, *Acta Polym.* **1989**, *40*, 243.
[42] E. N. Brown, M. R. Kessler, S. R. White, N. R. Sottos, *J. Microencapsul.* **2003**, *20*, 719.
[43] L. Yuan, G. Liang, J. Q. Xie, L. Li, J. Guo, *Polymer* **2006**, *47*, 5338.
[44] R. A. Prasetya, W. Hasokowati, *Am. J. Applied Sci.* **2010**, *7*, 739.
[45] D. G. Shchukin, M. Zheludkevich, K. Yasakau, S. Lamaka, M. G. S. Ferreira, H. Möhwald, *Adv. Mater.* **2006**, *18*, 1672.
[46] R. N. Wenzel, *Ind. Eng. Chem.* **1936**, *28*, 988.
[47] A. B. D. Cassie, S. Baxter, *Trans. Faraday Soc.* **1944**, *40*, 546.

ADVANCED FUNCTIONAL MATERIALS

Supporting Information

for *Adv. Funct. Mater.,* DOI: 10.1002/adfm.201401473

A Versatile Approach towards Multifunctional Robust Microcapsules with Tunable, Restorable, and Solvent-Proof Superhydrophobicity for Self-Healing and Self-Cleaning Coatings

*Gang Wu, Jinliang An, Xiu-Zhi Tang, Yong Xiang, and Jinglei Yang**

Supporting Information

Versatile Approach towards Multifunctional Robust Microcapsules with Tunable, Restorable, and Solvent-Proof Superhydrophobicity for Self-Healing and Self-Cleaning Coatings

Gang Wu,[†,‡] Jinliang An,[†] Xiuzhi Tang,[†] Yong Xiang,[‡] and Jinglei Yang[*,†]

[†]School of Mechanical and Aerospace Engineering, Nanyang Technological University, Singapore, 639798

[‡]School of Energy Science and Engineering, University of Electronic Science and Technology of China, Chengdu 610064, China

[*] Corresponding author email: mjlyang@ntu.edu.sg

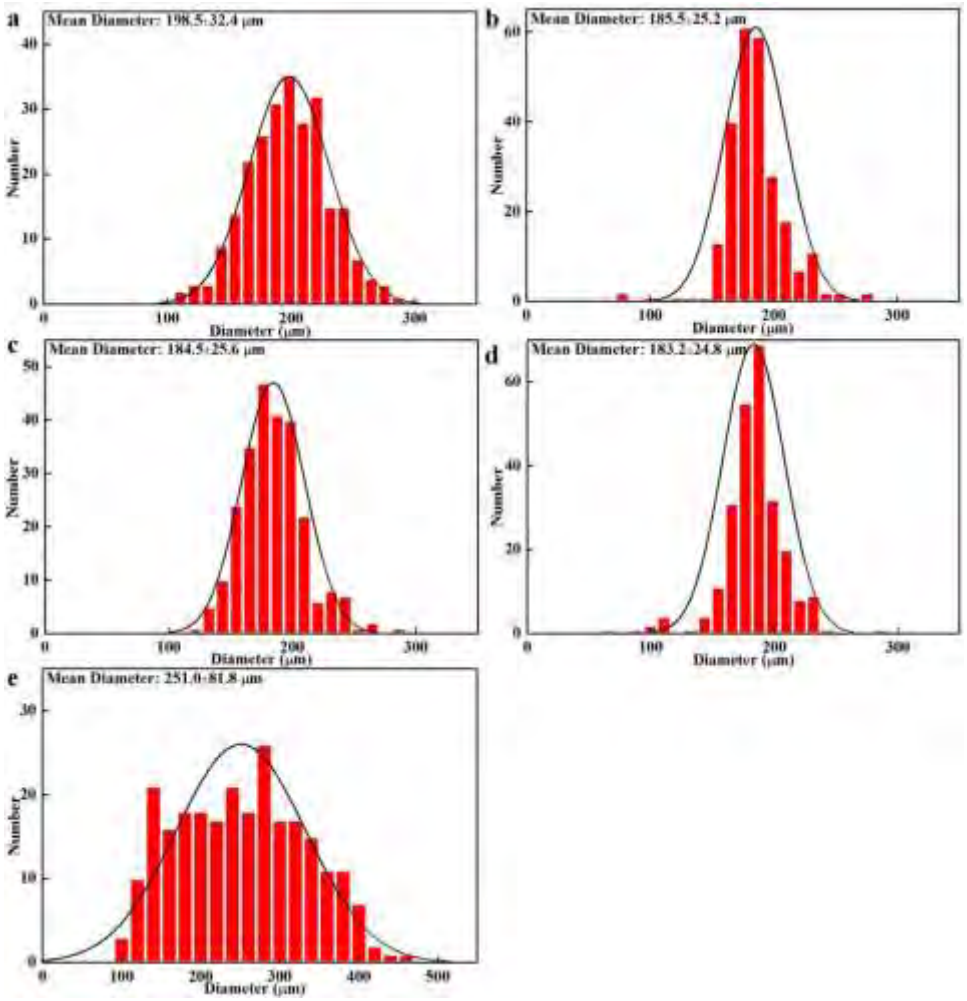

Figure S1. Diameter distributions of MCs with various cores: (a) HDI-MCs, (b) POTS-MCs, (c) Wax-MCs, (d) Xylene-MCs, and (e) HDI-D-MCs. The histograms of MCs diameter distribution were determined from 250 MCs statistic data of SEM images for each sample. The standard normal distribution curves were overlaid with the data (black solid line).

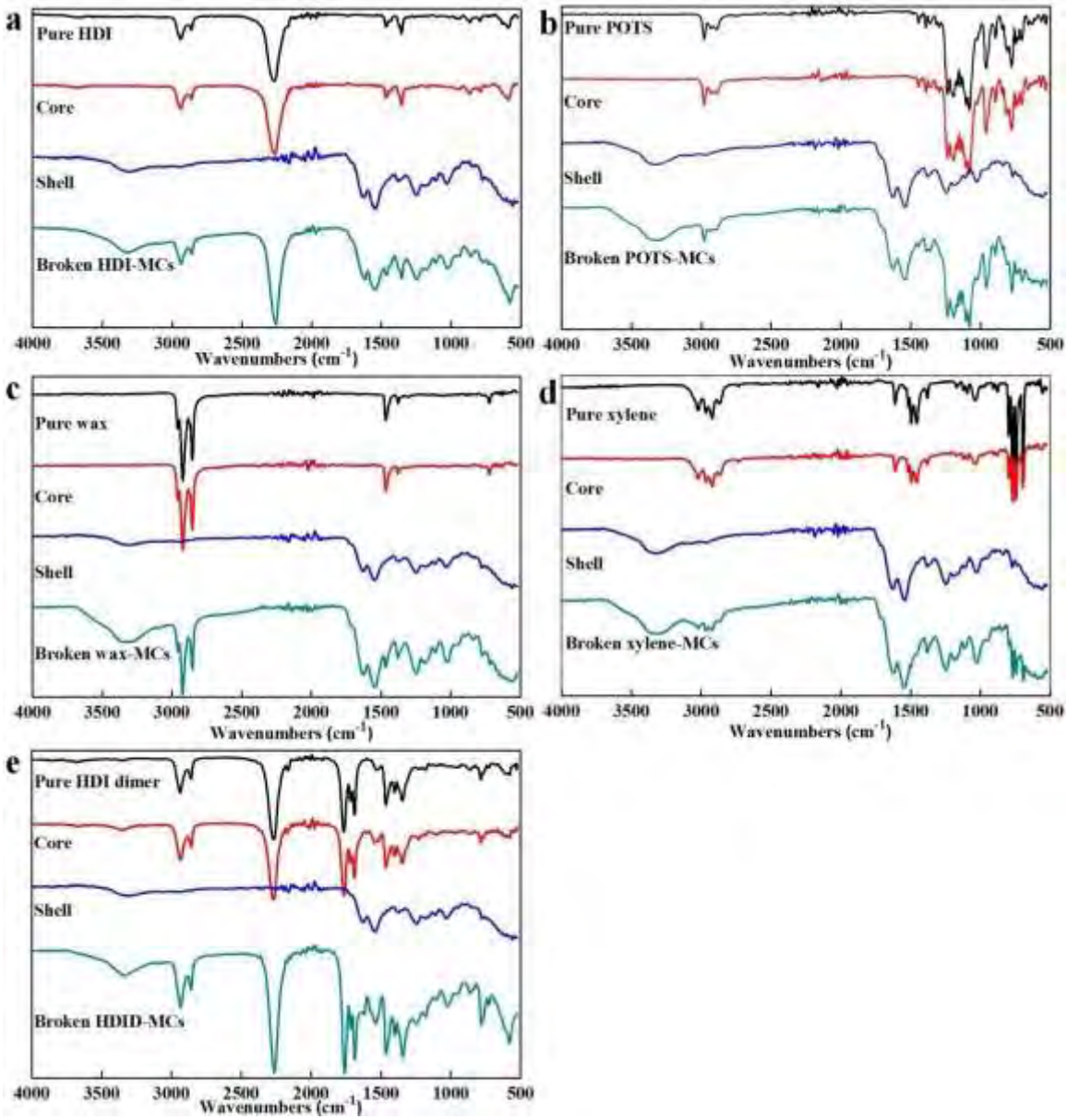

Figure S2. FT-IR spectra of different MCs with various cores: (a) HDI-MCs, (b) POTS-MCs, (c) Wax-MCs, (d) Xylene-MCs, and (e) HDI-D-MCs. For pure shell and core, small amounts of MCs were crushed and washed by acetone for 5-7 times. After filtration and drying, pure core and shell was obtained for analysis.

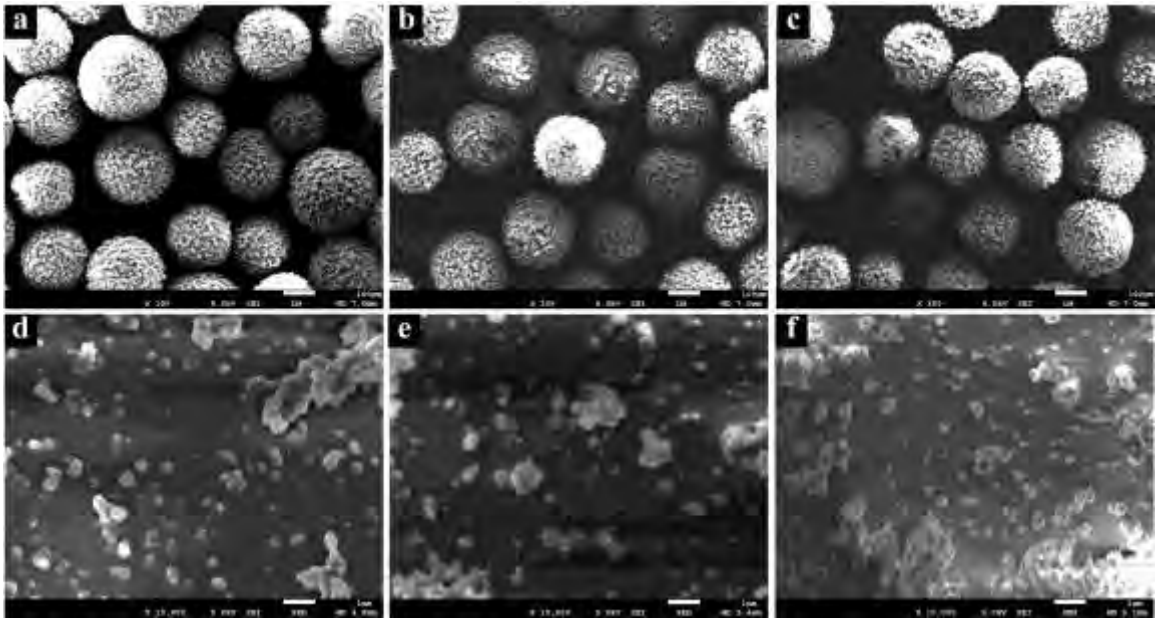

Figure S3. SEM images of dry HDI-MCs after 16 days immersion in different solvents: (a,d) in xylene, (b,e) in n-hexane, and (c,f) in chloroform.

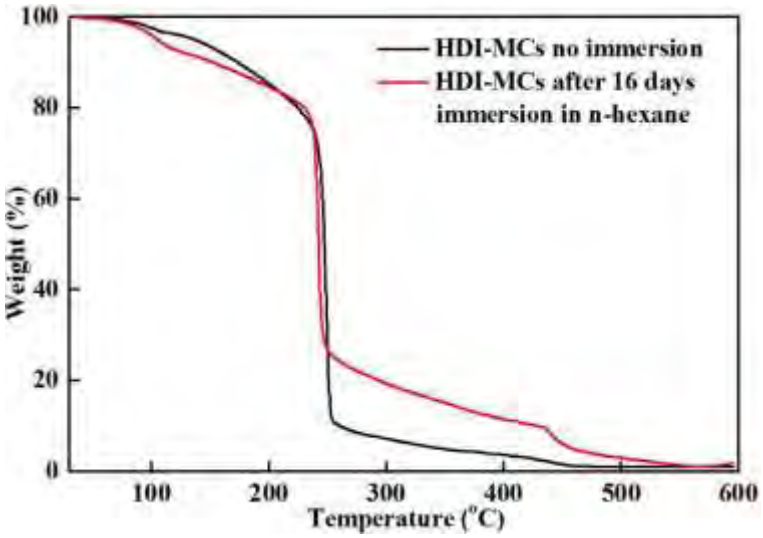

Figure S4. TGA weight loss curves of HDI-MCs no immersion in any solvent (black), HDI-MCs after 16 days immersion in n-hexane (red).The testing conditions were 10 °C min^{-1} of heating rate in N_2 atmosphere.

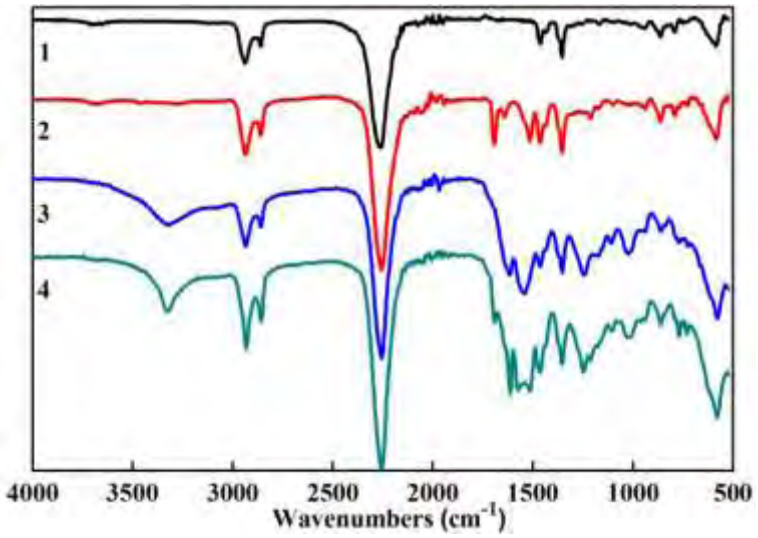

Figure S5. FT-IR spectra: (1) core of HDI-MCs after 0 day storage, (2) core of HDI-MCs after 45 days storage, (3) broken HDI-MCs after 0 day storage, (4) broken HDI-MCs after 45 days storage.

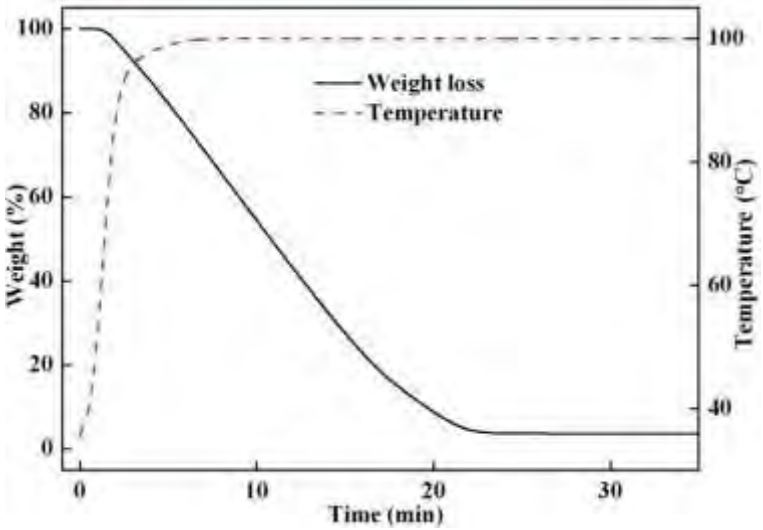

Figure S6. TGA weight loss curve of pure HDI in an isothermal process under 100°C (the solid line is weight loss as a function of time; the dash line is temperature as a function of time).

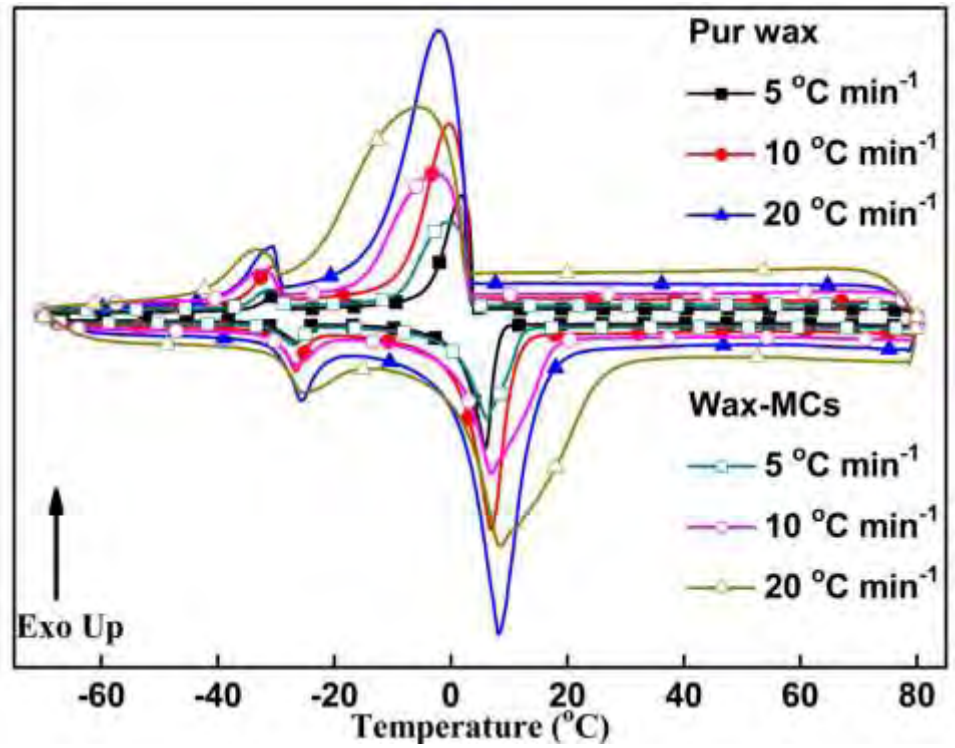

Figure S7. DSC curves of pure wax and Wax-MCs at different heating and cooling rates (heating rates are 5, 10, and 20 ^{0}C min^{-1}, respectively).

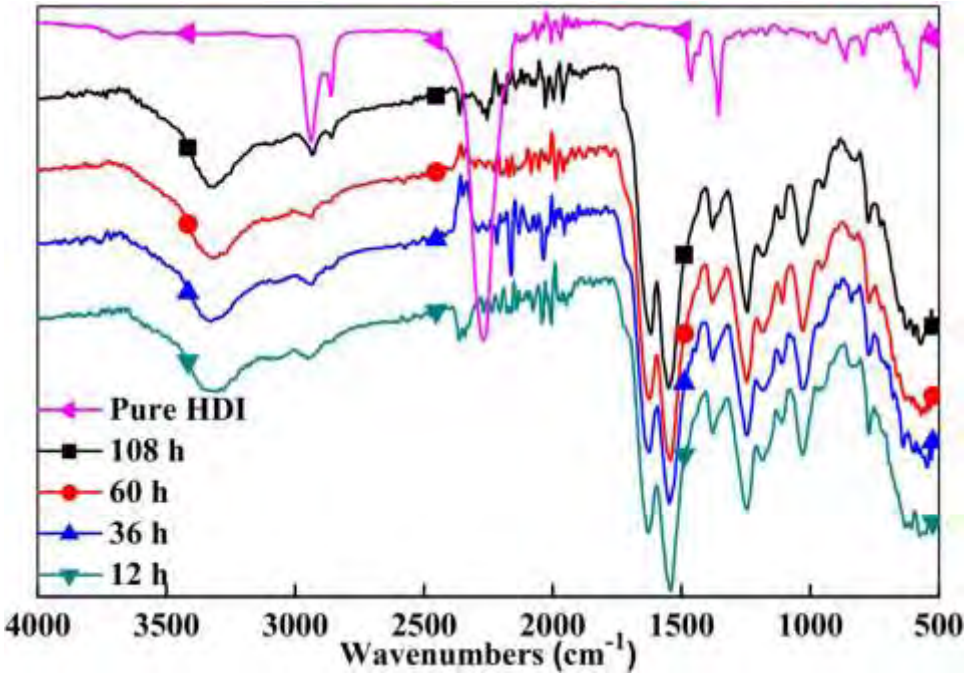

Figure S8. FT-IR spectra of the pure HDI and the HDI-MCs shell after aging 12 h, 36 h, 60 h, and 108 h, respectively.

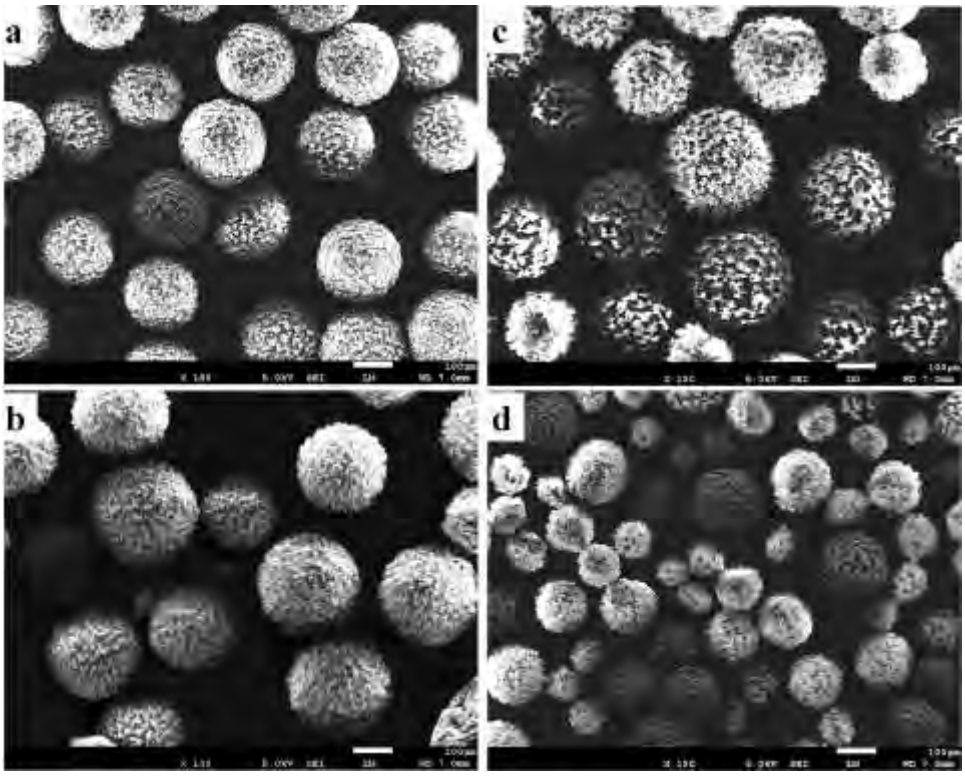

Figure S9. SEM images of HDI-MCs with different structures: (a) l-HDI-MCs, (b) m-HDI-MCs, (c) h-HDI-MCs, and (d) s-m-HDI-MCs.

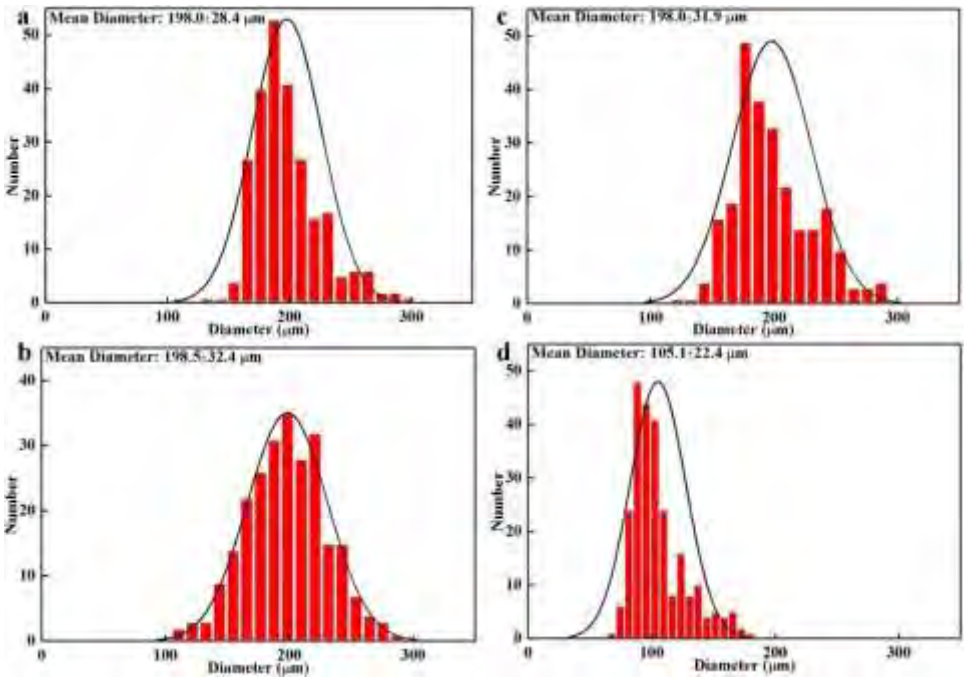

Figure S10. Diameter distributions of MCs with different structures: (a) l-HDI-MCs, (b) m-HDI-MCs, (c) h-HDI-MCs, and (d) s-m-HDI-MCs. The histograms of MCs diameter distribution were determined from 250 MCs statistic data of SEM images for each sample. The standard normal distribution curves were overlaid with the data (black solid line).

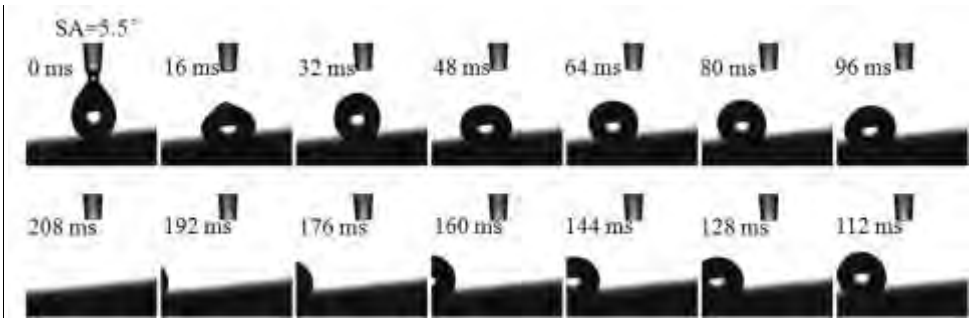

Figure S11. Sliding experiment of a water droplet (10 μL) on the surfaces of multifunctional coating with steel panel substrate. The sliding angle (SA) is 5.5°.

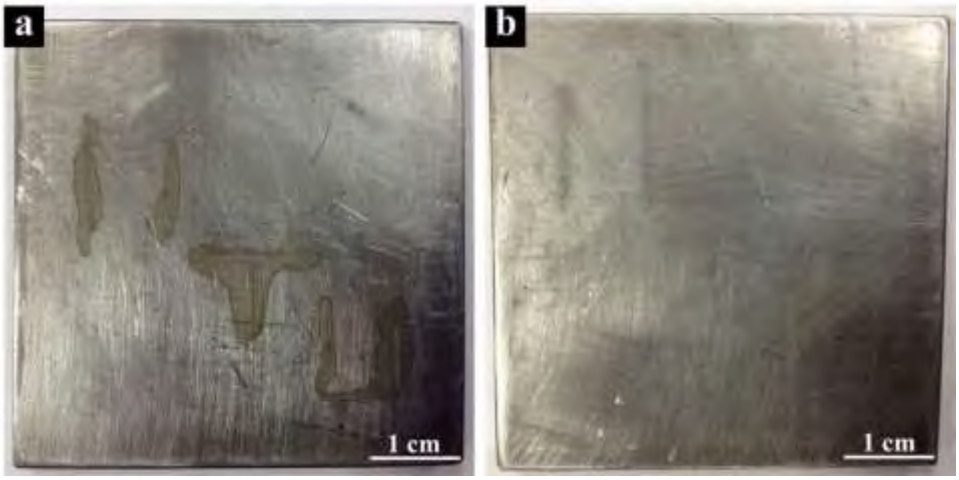

Figure S12. Photos of self-healing anticorrosion experiment. The steel panels peeled off coating after 48 h immersion: (a) for pure epoxy coating; (b) for HDI-MCs-embedded/bound epoxy coating.

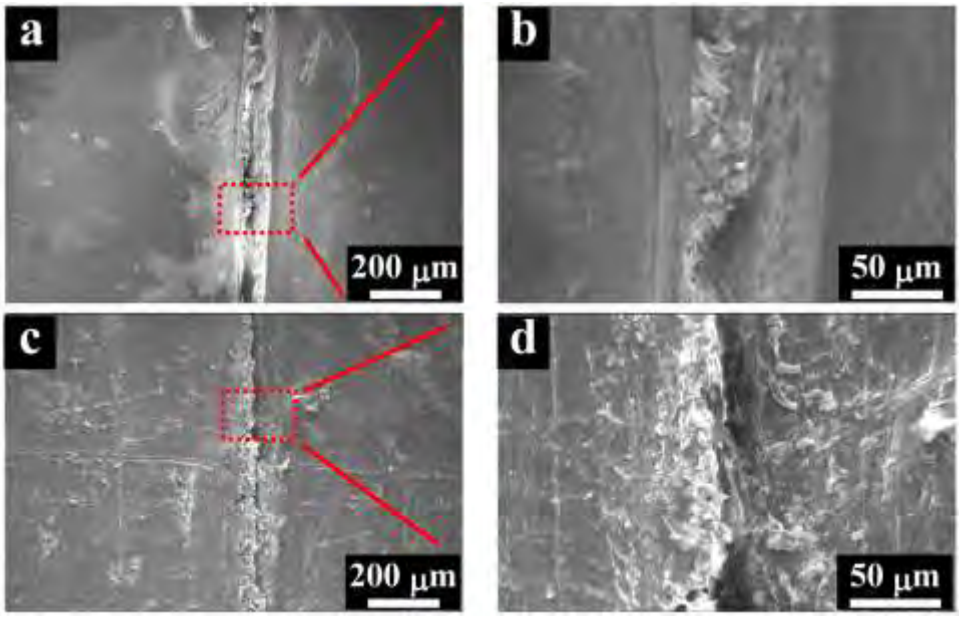

Figure S13. SEM images of scribed regions of the self-healing coating after 48 h immersion: (a,b) on top surface, (c,d) on bottom surface of coating.

Table S1. DSC data of pure wax and Wax-MCs.

Sample	Heating rate (^{0}C min^{-1})	Melting range (^{0}C)
wax	5	12
	10	17.5
	20	25
Wax-MCs	5	16.6
	10	23.6
	20	37.6